2005. Carpenter, K. (ed). The Carnivorous Dinosaurs. Bloomington, Indiana University Press.

17. Evidence for Predator-Prey Relationships

Examples for *Allosaurus* and *Stegosaurus*

KENNETH CARPENTER, FRANK SANDERS, LORRIE A. MCWHINNEY, AND LOWELL WOOD

Abstract

Unequivocal evidence of predator-prey relationships in the vertebrate fossil record is rare owing to the vagaries of preservation and the difficulties of interpretation. Occasionally, commutative evidence may be found that strongly implies such a relationship. Several pathological, contemporaneous specimens of the large theropod *Allosaurus* and the large stegosaur *Stegosaurus* from the Upper Jurassic Morrison Formation suggest an antagonistic relationship that is most likely between predator and prey. The specimens include a *Stegosaurus* cervical plate with a bite pattern that matches that of an *Allosaurus* mouth, an *Allosaurus* anterior caudal with a partially healed wound congruent with what a *Stegosaurus* tail-spike puncture would be expected to cause, and *Stegosaurus* spikes with broken tips exhibiting remodeling of the bone, implying that the spikes were broken well before death.

In this study, the spike force levels generated by the tail motion of *Stegosaurus* are estimated and compared to the stress levels likely to fracture the spikes. Tail spikes were susceptible to failure when imposed stresses exceeded their bending strength at impact or when shear or torsion loads exceeded spike strength. Estimates of spike penetration performance below load-induced failure levels at plausible spike-strike speeds and geometries suggest that life-threatening wounds could have

been imposed on a fully grown *Allosaurus*, as well as other predators and even conspecifics. The spike-bearing tail of *Stegosaurus* thus appears to have been a formidable weapon for both offensive and defensive purposes and may have contributed to the prolonged, widespread success of the stegosaurid taxon in the presence of the allosaurid one.

Introduction

Imputing behaviors to extinct organisms is difficult, especially when such behavioral hypotheses are untestable. Thus, analogies with the behaviors of living creatures are often cited to support particular hypotheses. When such analogies are not available, inductive reasoning may be presented, although such interpretative endeavors are even more hazard prone unless tested with pertinent models. Mechanical (Farlow et al. 1976) and computer (Myhrvold and Currie 1997) models have been used to test various hypotheses about behavior in dinosaurs, although the applicability of the models, and thus their results, can be open to question (e.g., Carpenter 1998a). Even the currently highly regarded phyletic bracketing must be employed with great caution. For example, Witmer (1995) used phyletic bracketing to suggest that ornithischians did not have cheeks. Whereas it is true that many birds and crocodilians do not have cheeks, their presence in ornithischians has been argued on morphological grounds (Galton 1973), on the basis of features not seen in any extant bird or crocodile. Furthermore, fleshy cheeks are present in the extant condor (Gregory Paul, pers. comm.), thereby negating the use of phyletic bracketing in this instance.

Only when direct evidence involving a specific behavior is preserved in the fossil record can a hypothesis be considered to have been adequately tested (Boucot 1990). For example, predator-prey interaction between two dinosaurs is documented in the famous pair of "fighting dinosaurs" of Mongolia: a *Velociraptor* with the sickle claw of its left foot extended in the neck region of a *Protoceratops*, and its right ulna and radius held within the *Protoceratops*'s beak (Carpenter 1998b). The close association between the two taxa has what Boucot (1990) referred to as a Category 1 behavioral-inference reliability. Because many of Boucot's (1990) categories are specific to invertebrates, a modified classification is presented in Table 17.1 that is specific to dinosaurs.

Some behavioral activities can result in trauma-related injuries on the skeleton. For example, Cott (1961) reports high instances of jaw injuries in extant crocodilians engaged in intraspecific combat, and similar injuries are known from the crocodilian fossil record (Buffetaut 1983). Paleopathological evidence for predation (vs. scavenging) by a theropod is very rare, with only one unequivocal example known: that of a hadrosaur, *Edmontosaurus*, that survived an attack dorsally on its mid-tail by *Tyrannosaurus* (Carpenter 1998b). This example also serves as evidence of Category 4 reliability for predator-prey interaction between two antagonists during the Late Cretaceous. Pathological specimens (described below) that are even older than the *Edmontosaurus* specimen provide evidence of comparable reliability for predator-prey

TABLE 17.1

Behavioral Reliability Categories for the Dinosaurian Record (adapted from Boucot 1990)

Category	Definition	Example	Reference
1	Organisms "frozen" in their interactions	Fighting dinosaurs of Mongolia; parental care of egg clutch by *Oviraptor*	Carpenter 1998b; Clarke, J. et al. 1999
2A	Organisms in close association implying behavior	Ceratopsian bonebed imply herding	Currie and Dodson 1984
2B	Functional morphology by direct comparison of extant organisms	Biomechanics of the caudofemoralis in theropods	Gatsey 1990
3	Evidence of behavior where the identity of the maker can be inferred with certainty	Embryos within eggs indicates that *Megaloolithus* eggs were laid by sauropods	Chiappe et al. 2001
4	Trace evidence of behavior where the identity of the maker is inferred, but not established conclusively	Healed bite mark on the caudals of *Edmontosaurus* by a large theropod (probably *Tyrannosaurus*)	Carpenter 1998b
5	Behavioral interpretation based on phyletic bracketing	Parental care (of sorts) must occur in dinosaurs because of care in extant crocodiles and birds	Horner 1997
6	Behavior for which interpretation is speculative, although reasonable	Thick domes of pachycephalosaurs implies flank butting	Carpenter 1997
7	Behavior so highly speculative as to have little reliability	Tail club of *Euoplocephalus* mimics the head so as to draw predators towards the wrong end	Thulborn 1993

interactions between two Late Jurassic candidate antagonists, the large theropod *Allosaurus* and the somewhat more massive stegosaurid *Stegosaurus*. All of the specimens are from the Upper Jurassic Morrison Formation.

Institutional Abbreviations. DMNH, Denver Museum of Nature and Science (formerly Denver Museum of Natural History); UMNH, Utah Museum of Natural History; UUVP, University of Utah, Vertebrate Paleontology collection.

Paleopathological Evidence

Example 1. Allosaurus *Caudal Vertebra*

Description. A caudal vertebra of *Allosaurus fragilis* (UMNH 10781; formerly UUVP 3811) (Fig. 17.1) was collected from the Cleveland-Lloyd Quarry, Emery County, Utah. The centrum is 11.5 cm long and 11.1 cm wide, suggesting that it is from a large individual of ~11 m total length. The left transverse process has a large hole measuring about 4 × 4.1 cm; its exact shape is difficult to characterize owing to

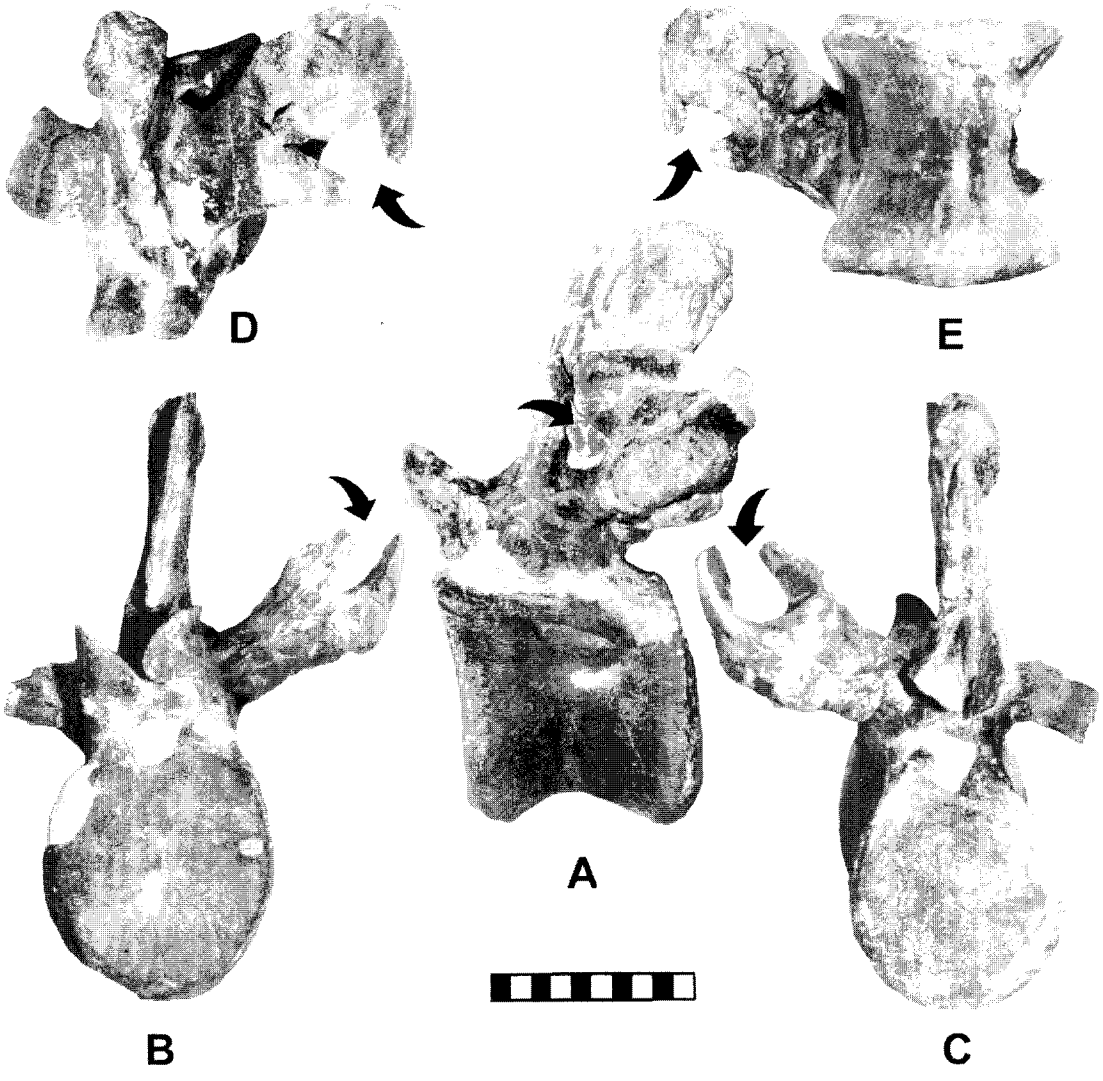

Figure 17.1. First caudal vertebra of Allosaurus fragilis *(UMNH 10781) showing a possible puncture in the caudal rib (arrow) in lateral (A), anterior (B), posterior (C), dorsal (D), and ventral (E) views. Scale in cm.*

pronounced dorsomedial reflection of the anterior portion of the transverse process. This hole opens into the distal edge of the process in an erupted, three-dimensional manner, generating an isthmus wound of roughly half the maximum diameter of the hole. This displaced process fragment has been frozen in its reflected position by remodeling of bone. The transverse process is extensively remodeled, especially on the ventral side as it attaches to the vertebral body. The surface of this remodeling displays a filigree pattern and a scattering of various-size matrix-filled openings. These openings appear to mark sinus tracts, for example, for the release of pus buildup within the underlying, severely distorted bone. Contralateral to this remodeling, on the ventral side of the transverse process, are several large, solid nodes formed by exuberant periosteal bone.

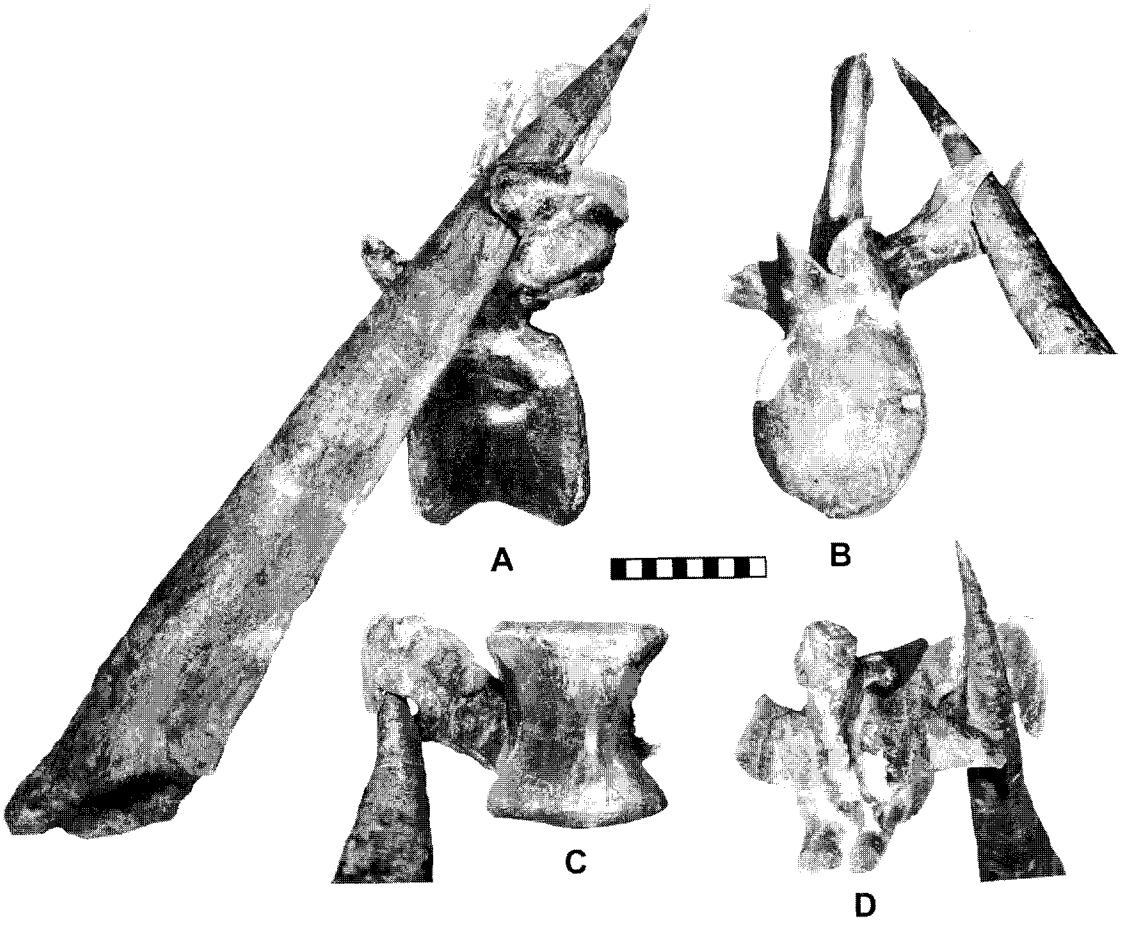

Figure 17.2. Supporting evidence that the puncture in the Allosaurus *caudal was caused by a* Stegosaurus *spike is seen by how well the spike fits within the pathology in lateral (A), anterior (B), ventral (C), and dorsal (D) views. When the spike pierced the caudal rib, it deflected a piece of bone upward as seen in B and D. Note in C the lobular periosteal reactive bone caused by bone infection and associated drainage sinuses for release of pressure caused by buildup of pus.*

Diagnosis. The pathological hole was caused by sharp-object trauma (the imposition of a piercing or penetrating object sufficiently forcefully as to mechanically fail the bone), as attested by a fragment of the transverse process that was reflected dorsomedially while the bone was still fresh (Fig. 17.2A,B,D). In addition, there is a ~0.5-cm-diameter, conical indentation in the transverse process located proximal to the hole itself. It is interpreted as the initial impact hole generated by the spike, which was then deflected sideways ~2 cm distally where it successfully created the main hole in the impacted process. The resulting hole is too large to have been formed by the tooth of any known Jurassic theropod. Furthermore, tooth punctures into bone leave distinct crush zones that record the shape of the tooth (Erickson and Olson 1996; Erickson et al. 1996), a shape that is distinct from the rounded, quite featureless shape of the hole in the *Allosaurus* process. Remodeling of the bone indicates that the wound was not immediately lethal. However, because little bone deposition occurred within the puncture, a substantial fragment of the spike may have broken off and remained lodged in the hole, where it mechanically blockaded bone deposition; or the animal may have expired before full remodeling could occur, for

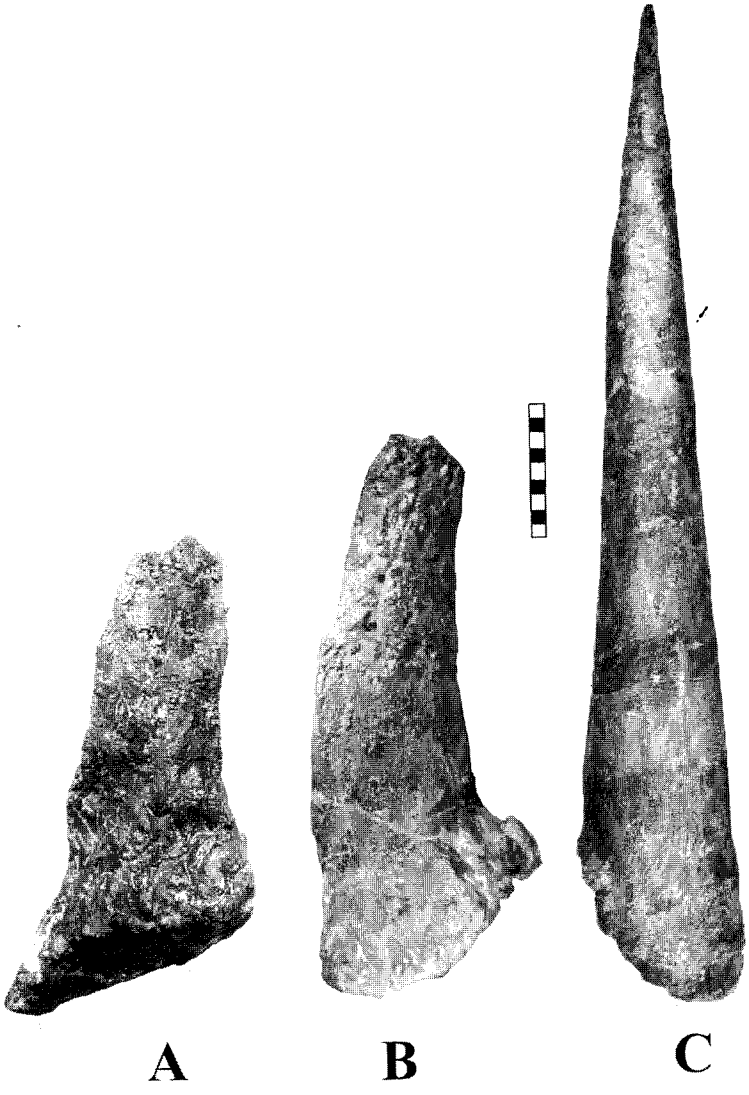

Figure 17.3. Stegosaurus *tail spikes broken in life and showing remodeling of the broken bone surface (A, DMNH 2212; B, USNM 6646) compared to a normal spike (DMNH 1483).*

example, from the systemic effects of wound infection. A more detailed description of the pathology will be presented elsewhere (Carpenter and McWhinney, in prep.).

Example 2. Broken Stegosaurus *Spikes*

Description. Several *Stegosaurus* tail spikes are known that have incomplete distal ends (Fig. 17.3). The truncated surfaces show remodeling of bone, indicating that the spike ends were lost significantly before the corresponding animals expired (McWhinney et al. 2001). The incidence of loss is interestingly high, appearing in 10 percent of the fifty-one specimens examined (though small-number statistics should be interpreted with caution). Although most specimens exhibited loss of at most a quarter of the distal portion of the spike, one specimen showed loss of a third of the estimated spike length.

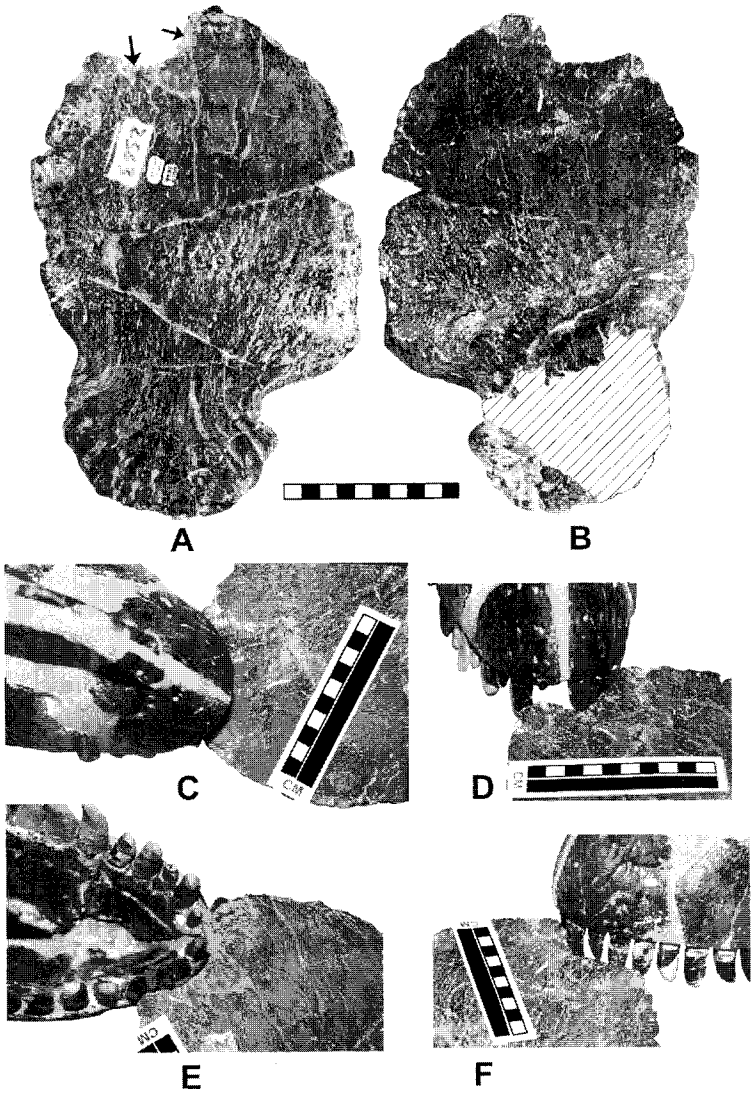

Figure 17.4. Possible bitten cervical plate of Stegosaurus *sp. (UMNH 5543) in lateral (A) and medial (B). Note the matrix still present along the inner edge (arrows) demonstrating that this damage occurred preburial. That this damage most likely was caused by an* Allosaurus *bite is seen in the multiple views of an* Allosaurus *skull in relation to the damage (C–F). Scale in cm.*

Diagnosis. The loss of the distal tip of the spike supports the hypothesis that the spikes were employed as defensive weaponry to initiate penetrating injuries that were sufficiently vigorous as to fail relatively high-strength bony structures. The remodeled surfaces show filigreed bone, rounding of the broken surfaces, and sinus tracks, all characteristic of post-traumatic chronic osteomyelitis (McWhinney et al. 2001). Estimates of the force levels necessary to fracture the spikes in this manner are presented below.

Example 3. Bitten Stegosaurus *Cervical Plate*

Description. A posterior cervical plate of *Stegosaurus,* which is characterized by the ventrolaterally flaring base (Carpenter and Miles, in prep.), shows a U-shaped notch along one of its distal edges. The plate (UMNH 5443), from the Cleveland-Lloyd Quarry, measures 28

cm in maximum height and 17.5 cm in greatest anteroposterior length. The U-shaped notch has a maximum width of 5.7 cm (Fig. 17.4A,B). That this damage preceded burial, collection, and preparation is attested to by the presence of matrix still adhering along the damaged section (Fig. 17.4A, arrows).

Diagnosis. The pattern of notching in this pathology dimensionally matches well the broad muzzle of a large *Allosaurus* (Fig. 17.4C–F), which argues for this animal's being the one that imposed this particular bite-type wound, rather than the more narrowly snouted *Ceratosaurus,* the other large theropod known from the Cleveland-Lloyd Quarry. For a variety of reasons, this plate damage is not likely to have been imposed postmortem via scavenging. First, the plates of *Stegosaurus* are believed to have consisted of skin overlaying bone, with no intervening muscle or viscera. Second, the geometric difficulty involved in accessing the plate when the *Stegosaurus* was lying dead, presumably on its side, with the distal edges of its plates drooping downward. Thus, the probable high ratio of bone to soft tissue and the noncongenial geometry suggest that the plate was likely to be of relatively low nutritive value and accessibility, further decreasing the likelihood of its being a scavenging target.

Interpretation

The examples of damage observed on several specimens of *Allosaurus* and *Stegosaurus,* both contemporaneous in the Morrison Formation, provide strong evidence for interspecific interaction between these two taxa. The large size and near-oval shape of the pathology in the caudal of the *Allosaurus* (Fig. 17.1) matches very well the cross-sectional geometry of a *Stegosaurus* spike (Fig. 17.2). On the basis of an empirically determined best fit, the spike pierced the transverse process from 58° below the horizontal plane, 33° anteriorly from the vertical transverse plane, and 10° laterally from the sagittal vertical plane. The spike apparently did not exit cleanly from the wound, as indicated by the anterior deflection of the transverse process fragment, as well as the tearing of an opening into its distal edge. This deflection of the bone may have resulted from the tip of the spike pivoting anteriorly relative to the vertebra, thus widening the hole. At this moment, the spike functioned as a first-class lever, with the motive force being provided by its inertia and by the *Stegosaurus* tail along the axis of the spike, applied at the spike base. The force applied to the *Allosaurus* transverse process was sufficient to deflect the fragment anteriorly and possibly resulted in the application of a shearing force sufficient to break off the tip of the spike. A fragment of the spike probably lodged in the wound hole because there is no evidence of bone deposition within the hole, though there is such on the outer surfaces. Such a spike fragment may have consisted primarily of the keratinous sheathing because its much lower mechanical strength (compared to the bone core of the spike) would result in its likely failure and fragmentation as the spike penetrated the process.

That *Stegosaurus* tail spikes did break off well before the deaths of

the individuals is evidenced by pathological spikes that quite unequivocally exhibit remodeling of fractured tips (McWhinney et al. 2001). As noted above, such damaged spikes occur in approximately 10 percent of the total spike sample, indicating that conditions for nonlethal tip-fracturing forces acting on spikes were not rare. The most probable forces included buckling, torsion, and shear: for example, when a spike underwent an axial impact on high-strength surfaces, such as pelvic structures, it would be subjected to forces down the axis of the spike (buckling); when a spike lodged and twisted about its axis, as it might in an *Allosaurus* caudal, it would be subjected to forceful, effectively rotational motion (torsion); and when a spike forcefully but obliquely struck a high-strength skeletal feature, it would be subjected to shear. Estimates of the stress levels needed to mechanically fail a tail spike in each of these three modes are developed below. Anticipating these results, we note that although spike penetration of soft tissues might sprain the regions where spikes were attached to *Stegosaurus* tails, only spike contact with mineralized tissues having intrinsic strengths comparable to the strength of spike bone is likely to fracture the spike itself in any of these three modes.

Further evidence of *Allosaurus-Stegosaurus* interaction is provided by what we have identified as a bitten cervical plate (Fig. 17.4). The neck of prey animals is a region typically attacked by large extant carnivores because several vulnerable structures occur there, including the trachea, carotids, and spinal cord (because of the relatively short neural spines and reduced muscle and tendon masses associated with comparatively low skull masses and moments). The existence of a bite-notched cervical plate in *Stegosaurus* supports the hypothesis that *Allosaurus* attacks did indeed occur on the neck. These plates, as well as the mosaic of ossicles surfacing the ventral portion of the *Stegosaurus* neck, may have served to defeat attacks aimed at tracheal crushing (Carpenter 1998a).

Stress Estimations and Force Analyses

The punctured *Allosaurus* vertebral transverse process and broken *Stegosaurus* tail spikes raise questions about the forces that the tail of *Stegosaurus* could have generated and transmitted to its tail spikes and about whether the corresponding stress levels were sufficient to mechanically fail the spikes and the transverse process in the manners described above. To answers these questions, we undertook two analyses: the first considers the force levels that may have been generated by the motions of the tail spike (Part 1), and the second considers the stress levels needed to mechanically fail the tail spikes in the three modes sketched above, as well as the stress levels required for the observed penetration of the vertebral transverse process (Part 2).

Part 1. Stegosaurus *Tail-Force Analysis*

Although the forces generated by *Stegosaurus* tail spikes cannot be directly measured, the forces can be analytically estimated within useful bounds. Such an analysis can be used in turn to estimate the amount

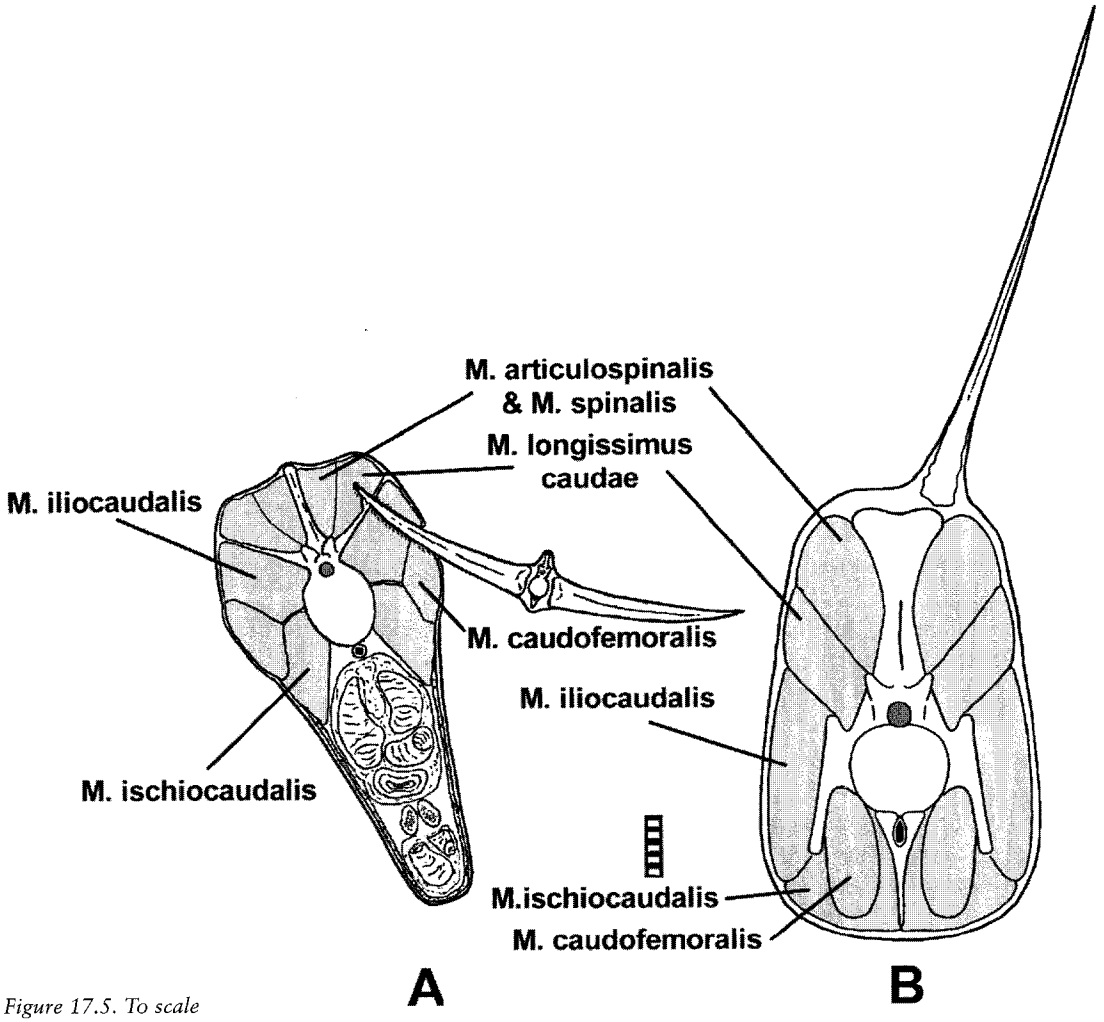

Figure 17.5. To scale reconstructions of the caudal muscles of Allosaurus *(A) and* Stegosaurus *(B) based on dissections of an adult* Caiman *sp. These illustrations are only aids to understanding* Allosaurus *and* Stegosaurus *as living creatures. In A, based on the position of the puncture in the caudal rib and angle of the puncture, the reconstruction suggests that the M. caudofemoralis, M. iliocaudalis, and M. longissimus caudae were pierced. The M. caudofemoralis is shown at its lateral position just before extending toward the fourth trochanter. In B, the muscle masses used to approximate the caudal strength in* Stegosaurus *are shown. Scale in cm.*

and type of damage that a *Stegosaurus* tail spike could have inflicted upon tissue and bone. This analysis is performed in two major parts. In the first part, the maximum striking force and related parameters are computed. In the second part, that force is compared to the force necessary to break two fossilized spikes that were damaged in life. The results of the analysis show that one of the spikes was probably broken as an immediate result of impact with a predator's body and that the second specimen must have been damaged as a result of having lodged in a predator's body (probably its skeleton) prior to being snapped in two as the two animals struggled to disengage themselves.

Two methods were used to calculate the force generated at the tip of the spike, and the results differ by about an order of magnitude. The more detailed approach yields the smaller value. Data for *Stegosaurus* are from a very large mounted skeleton, DMNH 1483. The spike used in the analysis has a length of 57 cm and a mid-shaft circumference of 17 cm (Fig. 17.3C).

TABLE 17.2

Estimated Range of Strength for Various Muscles in the Tail of *Stegosaurus*

Muscle	Cross-sectional area (cm^2)	Strength at 39 N/cm^2	Strength at 78 N/cm^2
M. articulospinalis and M. spinalis	200	7,800 N	15,600 N
M. longissimus caudae	200	7,800 N	15,600 N
M. iliocaudalis	225	8,800 N	17,600 N
M. caudofemoralis	200	7,800 N	15,600 N
M. ischiocaudalis	125	4,900 N	9,800 N
Total	950	37,000 N	74,000 N

Method 1

The first method assumes that the greatest amount of movement in the tail occurs near its base (Carpenter 1998a) and therefore that the proximal caudal muscles are the most important, especially the M. iliocaudalis, but also the M. articulospinalis, M. spinalis, M. caudofemoralis, and M. ischiofemoralis (Fig. 17.5B). This interpretation is supported by the vertically tall, cleat-like caudal ribs on the first ten to eleven caudal vertebrae for the M. iliocaudalis and their minimal development on the postcaudal eleven vertebrae. These tall caudal ribs leave little room for a large M. caudofemoralis, suggesting that this muscle was reduced relative to other dinosaurs in cross-sectional area (see Fig. 17.5B). Nevertheless, the muscle also contributed some force to the lateral movement of the tail by pulling against a statically held hind leg. The inferred force generated by these muscles can be approximated from their cross-sectional area, and the estimates range from 39 to 78 N/cm^2 (Ikai and Fukunaga 1968), although higher extremes (98 N/cm^2) have also been reported (Fick 1910). Using dissection of a modern adult caiman as a guide, the muscles were restored (Fig. 17.5B) to produce the muscle cross-sectional areas given in Table 17.2. Several of the cross-sectional areas are identical (numerical values were rounded to the nearest 5 cm^2). Muscle strengths based on the cross-sectional areas are also shown for the conservative force estimates of 4 kg/cm^2 and 8 kg/cm^2.

To determine the force at the tip of the spike at the moment of impact with the *Allosaurus* tail, the spike is treated as a slender cone (~10° full-angle), with the force concentrated at its tip. Two assumptions are made about the spike: first, that the keratin covering had a conservative thickness of 3 mm and, second, that *Stegosaurus* had no method of sharpening the tip of the spike the way a cat sharpens its claws. Therefore, in our model, the tip is slightly blunt rather than tapered to a point, with a conservative surface 6 mm in diameter and an area of 28 mm^2. The level of stress at the spike tip available for penetrating tissues may be estimated from momentum conservation

considerations. To move through a distance of 0.5 cm (taken to approximate the total cortical-bone thickness of the reference *Allosaurus* caudal vertebral transverse process) while uniformly decelerating by 10 percent, from a precontact speed V to a speed of $0.9V$, involves 20 percent of the spike's initial kinetic energy of $MV^2/2$, or $0.1MV^2$, where M is the spike's mass. This energy must be equal to a force, F, acting over a distance Dx (0.5 cm in this case): $F = (10^{-1})MV^2/Dx$, or $MV^2/5$ (we have adopted cgs units so that mass is in grams and force in dynes). The tail spike is estimated to have a mean density of 1.9 gm/cm^3 (based on the density of modern bone; Currey 2002). From the dimensions given above, its estimated volume is 2,150 cm^3, and its mass (sheathed with 3 mm of keratin) is about 4,000 gm. The mass of the entire end of the tail would be that of four spikes plus the connective tissue and the last few vertebrae, for a total of about 17,000 gm. The tail architecture of extant archosaurs supports tail-tip motion through a distance on the order of the animal's length within an interval on the order of 1 second, so that a characteristic maximum speed for the tail tip of a typical fully grown archosaur is on the order of the animal's length over 1 second of time (within, e.g., a factor of ~2, depending on the details of tail architecture). From this we estimate that the maximum speed, V, of an adult stegosaur's tail tip (and thus spike) likely was around 10 m/s, or 10^3 cm/s (roughly 20 mph).

We adopted this as a reference tail-tip speed and scaled our various results from it. The force estimate for slowing a 14,000-gm tail end (Tables 17.3 and 17.4) by a reference 10 percent from a reference speed of 10 m/s over a reference 0.5-cm distance then is $F = MV^2/5 = (14{,}000)(1{,}000)^2/5$, or 2.8×10^9 dynes. Applied over the reference spike-tip area of 0.28 cm^2, this force represents a pressure of 11.2×10^9 dynes/cm^2, or 11.2×10^4 N/cm^2 (11,200 bars, ~160,000 psi). This force level is 10–13 times that measured (Erickson et al. 1996, fig. 17.2) as being required to drive a curved conical penetrator—a shape replicated in a *Tyrannosaurus* tooth simulator—through fresh cortical bone 0.25 cm thick. It is more than enough to penetrate successively the two layers of cortical bone of roughly this thickness facing the two sides of the *Allosaurus* transverse process and to generate the observed wound (considering that the diameter of the wound in the *Allosaurus* caudal vertebra transverse process is twice that of the simulated *Tyrannosaurus* tooth-puncture hole in the bovid ilium and that the required penetration force scales linearly with wound diameter).

In summary, a small fraction (~10%) of the maximum kinetic energy of a stegosaurid tail spike moving at the reference speed of 10 m/s likely suffices to generate stress levels at the spike tip that are adequate to penetrate the *Allosaurus* caudal vertebral transverse process to the observed extent. Even if the stegosaur tail tip were moving only half as fast—5 m/s—less than half of the kinetic energy of a single tail spike would suffice to generate the stress levels sufficient to cause the observed wound in the *Allosaurus* caudal vertebral process.

Because the shear strength of living cortical bone is conservatively ~100 MPa (10^4 N/cm^2; Currey 2002), the estimated impact force of the mass of even a single spike, much less the mass of the end of the tail, is

Figure 17.6. (opposite page) (A) Maximum lateral motion of the Stegosaurus *tail is constrained by the rigid plate along the dorsal surface, thus dividing the tail into a set of rigid links. The tail cannot move beyond the limits imposed by the plates, otherwise gaps (tears) would occur (arrows) in the skin. To maximize lateral tail motion and maintain large plate size (light dashed lines), the base of the plate tapers (see Carpenter 1998a for further discussion). (B) The base to the system of links is the hips. Articulation angles (θa–e) are relative to the mid-line of the pelvis for proximal segment (a) and relative to succeeding links for distal segment (b–e). The basic model is a set of five rigid links that are determined by the presence of four rigid dorsal plates and a set of tail spikes on the distal segment. Movement is constrained to a single degree of freedom, within the horizontal plane. Muscles apply motive torque at the five points of articulation along the tail. (C) Relative velocity of* Stegosaurus *tail spikes as a function of articulation angle. Maximum impact force occur when velocity is maximized at the half-angle (left or right) of articulation shown in B. (D) Growth in angular velocity (ω) along the* Stegosaurus *tail as a function of time. Adapted from Kreighbaum and Barthels 1985.*

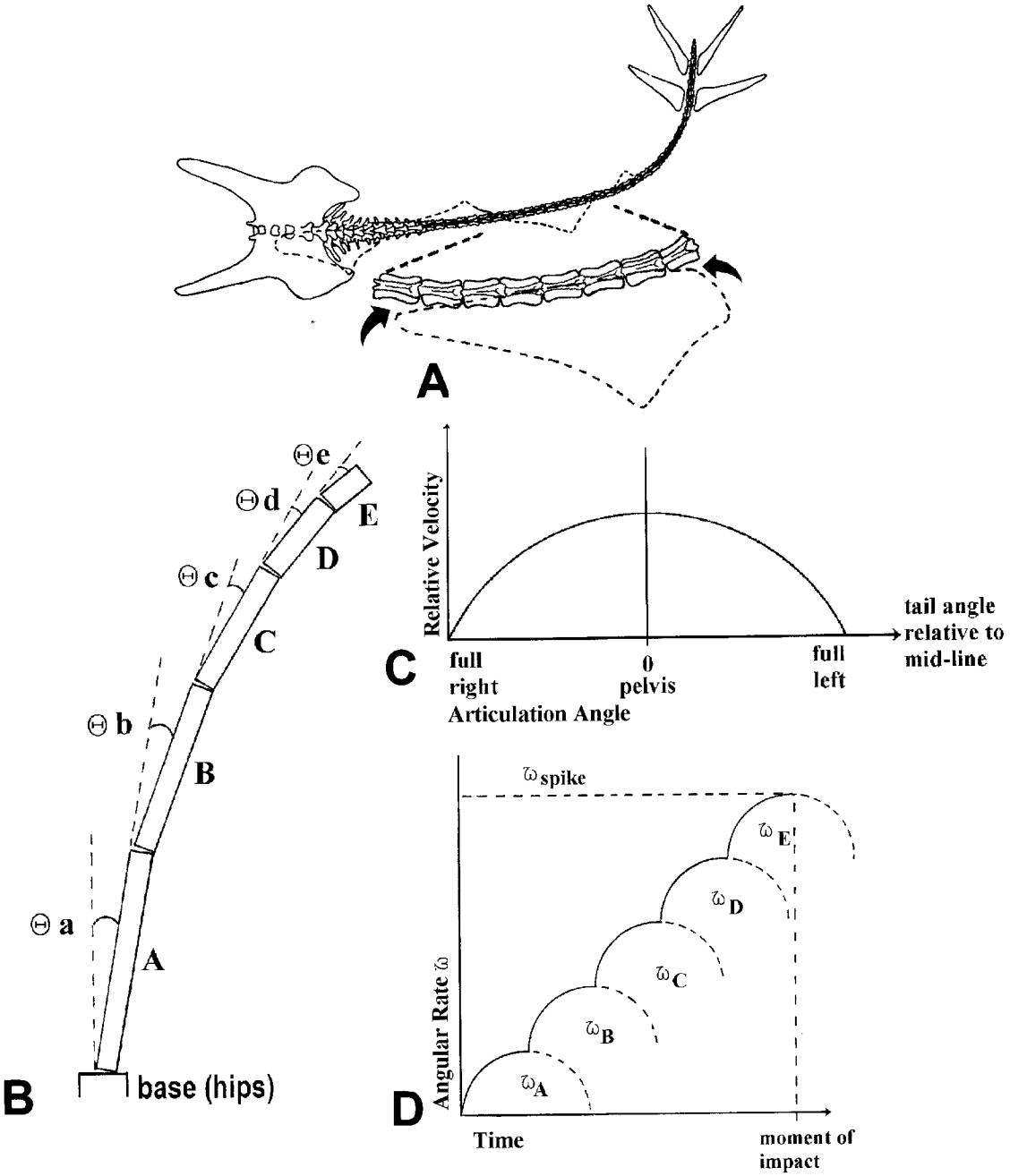

sufficient to break high-strength bone in shear. The impact-force estimate supports the basic reasonableness of our penetration estimates, as it is hundreds of times the amount necessary to penetrate soft tissues, and tens of times the minimum needed to crush thoracic cavities (and fracture gastralia) if applied over non-negligible fractions of their surfaces (Glasstone and Dolan 1977). It is several times the force that will potentially break the spike. Thus, if projected at reference speed against

likely target tissues, the "working tip" of a stegosaurid tail spike would not only penetrate and tear them, by large margins, but could also be mechanically threatened itself (if it were loaded predominantly in shear when it struck).

Method 2

The second method models the tail as a series of rigid links because of the constraints imposed by the dermal plates over large segments of the tail (Fig. 17.6A). Most movement can occur only where the plates do not overlap (Carpenter 1998a). The basic model (Fig. 17.6B) is a set of five rigid links that are determined by the presence of four rigid dorsal plates and a set of tail spikes on the distal segment. Movement is constrained to a single angle of medial-lateral movement in the horizontal plane. Muscles are assumed to apply motive torque at the five points of articulation along the tail. The maximum articulation angle available to each link is a critical parameter in the calculation of spike impact forces. *Stegosaurus* could have swung the tail laterally on both sides of the body (Fig. 17.6C); but for simplification, analysis is done with half-angles of articulation. Spike velocity would have necessarily dropped to zero at each end of a full-angle swipe (Fig. 17.6C).

Theoretical Analysis of Tail Motion. Each rigid link has rotational movement about its proximal point of articulation. The rotational equations of motion for each link are

$$L = I\omega, \text{ (angular momentum) (1a)}$$
$$T = I\dot{\omega} = |\vec{r} \times \vec{F}|, \text{ (torque) (1b)}$$

and

$$KE = \tfrac{1}{2} I\omega^2 \text{ (kinetic energy), (1c)}$$

where

I = moment of inertia ($kg \cdot m^2$);

ω = the link's rate of rotation (rad/s);

$\vec{r}$ = half-width at the base of each link; and

$\vec{F}$ = muscle force exerted at the base of each link.

For each link,

$$I = \int_{L1}^{L2} x^2 \rho dx = x^3 \Big|_{L1}^{L2} \left(\frac{\rho}{3}\right) = \frac{(L2^3 - L1^3)}{3}\rho \text{ , (2)}$$

where ρ is the segment's average mass density per unit length; $L1$ and $L2$ are the distances from its proximal and distal ends, respectively, to the base of the tail; and x is the variable of integration between $L1$ and $L2$ along the link. Plate mass and moment are considered to be negligible compared to the mass and moment of other link tissues and bone.

Note that the angular momentum and kinetic energy (Eqs. 1a, 1c) of a link are measures of its state of motion. But the motive torque, $T = |r \times F|$ (Eq. 1b), is derivable from the tail's physical characteristics and the performance of modern muscle. Torque is generated at the proximal end of each link by muscle contraction. The torque available at the proximal end of each link is

$$T = (A_{\text{cross-section}}) \times (F_{\text{muscle}}) \times \left(\frac{W_{\text{link}}}{2}\right), \quad (3)$$

where $A_{\text{cross-section}}$ is the total area of cross-sectional muscle, F_{muscle} is the force the muscle can exert per unit cross-sectional area, and W_{link} is the width of the link. The factor of $^1/_2$ in Eq. 3 is required because only half of the muscles at the base of each link (those on the side toward which the tail is swinging) can apply pulling (torquing) force. The other half must elongate and can apply only minor torque that stabilizes, controls, or both.

The impact force generated by a tail spike is related to the spike's velocity during the impact and to the mass of the link to which the spike is attached. Other physical parameters related to the impact, such as maximum pressure applied, are also derivable. The key to deriving all these quantities is to determine the angular rate of movement, ω, of the spike at the moment of impact. As the *Stegosaurus* tail swings laterally, ω should add from one link to the next as shown in Figure 17.3.

The angular rate of the tail spike equals the sum of the maximum angular rates of each link in Figure 17.1:

$$\omega_{\text{spike}} = \omega_A + \omega_B + \omega_C + \omega_D + \omega_E. \quad (4)$$

Each ω must in turn be related to the physically measurable or derivable quantities of *I*, *T*, and the angle through which the corresponding link moves, θ. Conversion to these quantities is done mathematically as follows:

$$\omega = \dot{\theta} = \int \dot{\omega} dt = \dot{\omega} t \quad (5a)$$

$$\theta = \iint \dot{\omega} dt = \int \dot{\omega} t = \frac{\dot{\omega} t^2}{2} = \frac{\omega t}{2}. \quad (5b)$$

From Eq. 5b, ω is related to θ and to time, *t*, as

$$\omega = \frac{2\theta}{t} = \dot{\omega} t. \quad (5c)$$

Rearranging algebraically yields

$$t^2 = \frac{2\theta}{\dot{\omega}}. \quad (5d)$$

Substituting for ω (from Eq. 1b) yields

$$t^2 = \frac{2\theta I}{T} \quad (5e)$$

and

$$t = \sqrt{\frac{2\theta I}{T}}. \quad (5f)$$

Substituting Eq. 5f for *t* into Eq. 5c yields ω in terms of θ, *T*, and *I*:

$$\omega = \sqrt{\frac{2\theta T}{I}}. \quad (5g)$$

Equation 5g can be used to represent the individual terms in Eq. 4 as follows:

$$\omega_{\text{spike}} = \sqrt{\frac{2\theta_A T_A}{I_{\text{tail}}}} + \sqrt{\frac{2\theta_B T_B}{I_{\text{tail-A}}}} + \sqrt{\frac{2\theta_C T_C}{I_{\text{tail-A-B}}}} + \sqrt{\frac{2\theta_D T_D}{I_{\text{tail-A-B-C}}}} + \sqrt{\frac{2\theta_E T_E}{I_{\text{tail-A-B-C-D}}}} \quad (6)$$

TABLE 17.3.

Measured Values for *Stegosaurus stenops* Tail (DMNH 1438)

Link	Length (cm)	Height (cm)	Width (cm)	Plate base length (cm)	Plate height (cm)	Maximum width at base (cm)	Half-angle of articulation (deg, radians)
A	100	50	18	70	75	5	4, 0.070
B	63	32	13	64	64	6	2.3, 0.040
C	41	26	9	34	31	4	2.8, 0.049
D	37	20	7.5	28	24	5	3.1, 0.054
E	69	11.5	7	9*	50*	n/a	1, 0.017

*For Link E, the plate base length and plate height parameters refer to the base diameter and length, respectively, of a spike.

The moments of inertia range from that of the entire tail in the first term to that of the most distal link in the last term.

The value of Eq. 6 for the spike's angular rate is converted into force by first converting it to linear spike velocity, V_{spike}:

$$V_{spike} = (L_{tail} \cdot \omega_{spike}), \quad (7)$$

where L_{tail} is the length of the tail from the proximal end of link A to the distal end of the spike.

Assuming that the spike halts inside the target tissue and bone, the impulse delivered by the spike, P_{spike}, is

$$P_{spike} = (m_E \cdot V_{spike}), \quad (8)$$

where m_E is the mass of the distal tail link. The pressure exerted by the spike on the target is this impulse divided by the surface area of the spike tip:

$$Pressure_{spike} = \frac{P_{spike}}{A_{spike\ tip}} . \quad (9)$$

Measurements and Analysis of Stegosaurus stenops *Tail.* The measurements, taken at the distal end of each link in the *Stegosaurus* tail, included the height and width of the vertebral structures (including transverse processes, chevrons, and neural spines) and the half-angles of articulation (Fig. 17.6B). The articulation half-angles were directly measurable because the tail is mounted nearly at its maximum possible articulation. Dorsal plates were measured for base length, height, and maximum width at the base. Spikes were measured for length and base diameter. Measurements are summarized in Table 17.3.

The cross-sectional area of each link was calculated as the arithmetic mean of the ellipsoidal and parallelogram areas implied by the heights (H) and widths (W) in Table 17.3. Ellipsoidal area is given by

$$A_{ellipsoidal} = \pi \left(\frac{\left(\frac{H}{2}\right)^2 + \left(\frac{W}{2}\right)^2}{2} \right) \quad (10)$$

and parallelogram area by

TABLE 17.4

Summary of Volume and Mass for *Stegosaurus stenops* Tail (DMNH 1438)

Link	Cross-sectional area(cm^2)	Bone ($\rho = 1.98$) to muscle ($\rho = 1.0$) ratio	Nonplate mass per unit length (gm/cm)	Total cross-section muscle area(cm^2)	Link length (cm)	Cross-sectional unit length mass × length(kg)	Plate volume (cm^3)	Plate volume × bone density = mass(kg)	Total link mass(kg)	Total mass per unit length (gm/cm)
A	780	1:3	971	585	100	97	4,375	8.7	106	1,060
B	338	1:2	448	225	63	28	4,096	8.1	36	571
C	207	1:1	308	104	41	12.6	703	1.4	14	341
D	127	1:1	189	64	37	7.0	560	1.1	8	216
E	56	1:1	83.4	28	69	5.8	4,240*	8.4*	14	203

*The volume of a single spike (1,060 cm^3) and the mass of a single spike are multiplied by four to yield total spike volume (4,240 cm^3) and total spike mass (8.4 kg).

TABLE 17.5

Link Torques and Moments of Inertia

Link	Muscle cross-sectional area(cm^2)	Force range (half of muscle cross-section multiplied by 39 N/cm^2 to 78 N/cm^2 (N)	Link half-width, r (m)	Torque at base of link $\|r \times F\|$ (N·m)
A	585	11,400–22,800	0.09	1,000–2,000
B	225	4,400–8,800	0.065	285–570
C	104	2,000–4,100	0.045	91–182
D	64	1,250–2500	0.0375	47–94
E	28	550–1100	0.035	19–38

TABLE 17.6

Link Moments of Inertia

Link	Unit length density (Table 17.4) (gm/cm)	I_{tail} ($kg \cdot m^2$)	$I_{tail\text{-}A}$ ($kg \cdot m^2$)	$I_{tail\text{-}A\text{-}B}$ ($kg \cdot m^2$)	$I_{tail\text{-}A\text{-}B\text{-}C}$ ($kg \cdot m^2$)	$I_{tail\text{-}A\text{-}B\text{-}C\text{-}D}$ ($kg \cdot m^2$)
A	1,060	35	n/a	n/a	n/a	n/a
B	571	63	4.8	n/a	n/a	n/a
C	341	47	9.9	0.78	n/a	n/a
D	216	40	12	2.9	0.36	n/a
E	203	107	44	18	7.7	2.2

$$A_{parallelogram} = \left(\frac{H \cdot W}{2} \right) . \quad (11)$$

Therefore, the mean cross-sectional area is each tail link is estimated to be

$$A_{cross\text{-}sectional} = \left(\frac{A_{ellipsoidal} + A_{parallelogram}}{2} \right) . \quad (12)$$

Plate volume is estimated to be the area of the equivalent triangle multiplied by $^1/_3$ the base width:

$$Volume_{plate} = \frac{Width}{3} \left(\frac{Base \cdot Height}{2} \right) = \frac{1}{6} \left(Base \cdot Height \cdot Width \right) , \quad (13)$$

and spike volume is derived from the formula for the volume of a cone:

$$Volume_{spike} = \frac{1}{3} \pi \left(\frac{d}{2} \right)^2 L , \quad (14)$$

where d is the base diameter and L is the length. Masses were calculated by multiplying the average tissue and bone density of each object with the volumes. The density of tissue is 1 gm/cm^3, and the density of bone is 1.98 gm/cm^3. Table 17.4 summarizes these values for volume and mass. Table 17.5 summarizes the calculation of motive torque (Eq. 3) and moment of inertia (Eq. 2) for each link. Based on modern muscle

TABLE 17.7

Link Angular Rates for Equation 6

Link	Torque at base of link sequence (Table 17.5) (N·m)	Cumulative moment of inertia (sum of columns in Table 17.6) (kg·θ·m²)	Half-angle of articulation (Table 17.4) (rad)	ω term (Eq. 6) (rad/s)	ω term (Eq. 6) (deg/s)
A+B+C+D+E	1,000–2,000	290	0.070	0.70–0.98	40–56
B+C+D+E	290–570	71	0.040	0.57–0.80	33–46
C+D+E	91–180	22	0.049	0.64–0.90	37–52
D+E	47–94	8.1	0.054	0.79–1.1	45–63
E	19–38	2.2	0.017	0.54–0.76	31–43

performance, the force exerted by muscles could range between 39 N/cm² and 78 N/cm². This performance range provides lower and upper bounds for this analysis.

Table 17.6 contains individual angular rates and the calculated moment of inertia terms that appear in Eq. 6. Note that the moment of inertia of the distal link is large because of the presence of the four spikes. This large moment of inertia produces a telling effect on the target.

Calculated Maximum Performance of the Tail in Stegosaurus. The sum in Eq. 6 is the sum of the ω values in Table 17.7. The range is 3.2–4.5 rad/s, depending upon the muscle force that can be brought to bear (as noted above). The total tail length is 3.1 m, but the last spike is 39 cm short of the end. Therefore the spike is 2.71 m from the proximal end of link A. From Eq. 7, the spike tip velocity is (assuming a spike radius of 2.71 m from the proximal end of link A):

$$(\omega_{spike} \cdot L_{spike}) = (3.2 - 4.5\text{rad/s}) \cdot (2.71\text{m}) = 8.7\text{–}12\text{m/s}. \quad (15)$$

In English units, the spike velocity range is 20–27 mph. This value brackets the estimate of 10 m/s (~20 mph) determined by Method 1, above.

Using a conservative value of 14 kg for the mass of the end of the stegosaur tail (Table 17.4), the impulse delivered to the target is given by Eq. 8:

$$P_{spike} = (14\text{ kg}) \cdot (8.7\text{–}12\text{m/s}) = 120\text{–}170\ \frac{\text{kg}\cdot\text{m}}{\text{s}}. \quad (16)$$

If the stopping time in the target tissue and bone is (conservatively) estimated to be about $^1/_3$ s, then the maximum force, *F*, exerted on the target (the impulse given in Eq. 16 divided by this interval) is

$$F_{max} = \frac{P_{spike}}{t_{stopping}} = \frac{120 - 170\ \frac{\text{kg}\cdot\text{m}}{\text{s}}}{\frac{1}{3}\text{s}} \approx 360 - 510\text{ newtons}. \quad (17)$$

The minimum calculated impact force of 360 N is more than adequate to damage bone and tissue struck by the *Stegosaurus* spike (see discussion under Method 1).

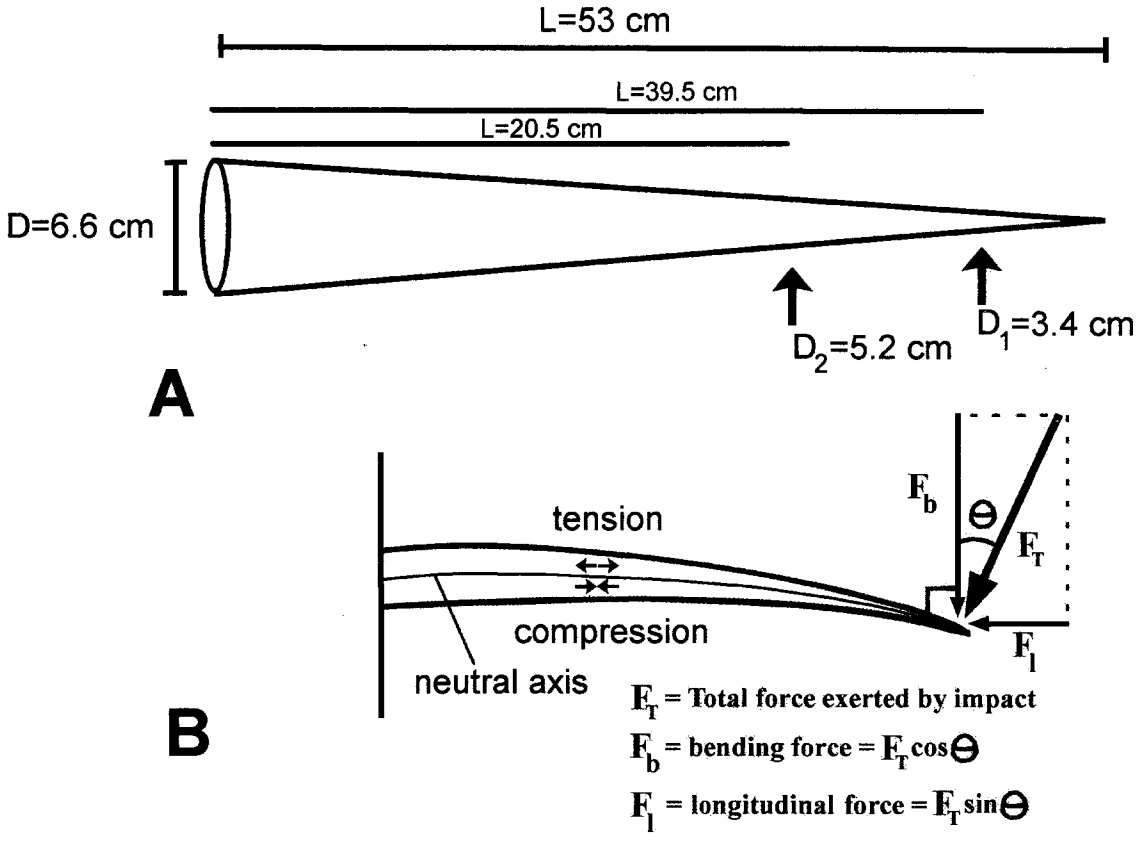

Figure 17.7. (A) Schematic illustration of a Stegosaurus *spike and values used to determine breakage at D_1 (based on USNM 6646) and D_2 (DMNH 2818). (B) Schematic of a* Stegosaurus *spike as a non-uniform cantilever with forces applied to it. The total impact force on the spike, F_T, is reduced to two components, one parallel to the spike's longitudinal axis and the second perpendicular to the first. The perpendicular component, F_b, tends to bend the spike through tension and compression on either side of a force-neutral central axis. If these stresses exceed the strength of the bone at some location along the spike, then the bone will break. The impulsive force application causes the bone to behave with only about 80 percent of the strength it would have if the force were applied gradually.*

Both methods of analysis for *Stegosaurus* indicate that the tail spikes could generate more than sufficient force to puncture the *Allosaurus* vertebra.

Part 2. Stegosaurus *Spike Breakage Force Analysis*

In the analysis of *Stegosaurus* spike pathologies, most specimens showed breakage near their tips, but one showed loss of the distal third (McWhinney et al. 2001). How much force was needed to cause these breaks, and are the results within the range of force the tail is estimated to have generated?

The breakage pattern of all the spikes indicates loading perpendicular to the long axis of the spike (Fig. 17.7). The broken surface is not long and oblique as would be seen when if loading were parallel to the axis (Currey 2002). Breakage could occur when the spike hit a hard object (e.g., bone) at an angle roughly perpendicular to the longitudinal axis of the spike, or when the spike had already penetrated deeply into the target body and torsion was applied by the struggling animal. Regardless, for the spike, the direction of forces is the same.

The spike is treated as a cantilevered beam with conical shape (of length L and base diameter D), as shown in Figure 17.7. (Actual spike cross-sections are slightly flattened, but the circular approximation simplifies the analysis and provides no significant change in the final

result.) The impact force, F, causes tension stress along one side and compression stress on the opposite side (Fig. 17.7B). These forces balance along the spike's center axis, or neutral line. The stress level varies along the length of the spike, increasing from the base to the tip as described below. If at any point the stress exceeds the strength of the bone, then the spike will break at that point.

The force vector that tends to bend the spike along its length (and which ultimately may break it), denoted F_b, is somewhat less than the total striking force, F_T. The two components are related by the cosine of the angular difference, θ, between the impact angle of F_T and 90° (which is the perpendicular to the spike's long axis):

$$F_b = F_T \cos\theta. \quad (18)$$

Although F_b is expected to be somewhat less than F_T, the swept-back angle of *Stegosaurus* spikes (about 65° relative to the tail centerline as shown in Figure 17.5) results in an impact angle of 65° for the case in which the attacker's body is parallel to the *Stegosaurus* body and the *Stegosaurus* tail hits with maximum force, just as it crosses the centerline of the *Stegosaurus* hips. This geometry suggests that *Stegosaurus* spikes must have ordinarily been used more for slashing than for spearing or stabbing. For this geometry,

$$\cos\theta = \cos(90°-65°) = \cos(25°) \approx 0.906. \quad (19)$$

Because the cosine of the difference angle (25°) is nearly unity, it is apparent that for this geometry F_b and F_T can be considered to be nearly equal. (At the end of this analysis, the factor of 0.906 in Eq. 19 will be taken into account.) In the remainder of this analysis, the force term that tends to bend the spike is thus rendered simply as F and is assumed to be nearly equal to the impact force of the spike. Also note that a spike might not be broken upon impact and might instead become embedded in target tissue or bone. In that case, the wrenching force exerted by the exertions of the two animals is likewise expected to be exerted at roughly right angles to the spike's longitudinal axis and can also be rendered simply as F.

Referring again to Figure 17.7, the diameter, d, of the spike at any length, l, measured from the base is

$$d(l) = D\left(\frac{L-l}{L}\right) = D\left(1-\frac{l}{L}\right), \quad (20)$$

where

D = spike diameter at the base; and

L = total spike length.

The moment of inertia, I, about any point is (from Eq. 2):

$$I = \frac{\pi d^4}{64} = \frac{\pi D^4 (1-l/L)^4}{64}. \quad (21)$$

The section modulus, Ω, is (from Eq. 2):

$$\Omega = \frac{2I}{d} = \frac{\pi d^3}{32} = \frac{\pi D^3}{32}\left(1-\frac{l}{L}\right)^3 = \frac{\pi D^3}{32} \bullet \frac{(L-l)^3}{L^3}. \quad (22)$$

TABLE 17.8

Force Necessary to Cause Spike Failure at Observed Lengths for Specimens 1 and 2

The correction in the last column is obtained from Equations 18 and 19.

Specimen number	$\kappa(m^2)$	$S_{critical}$ (Mpa)	$F_{applied} = \kappa S_{critical}$ (N)	$F_{total} = F_{applied} / 0.906$ (N)
1 (static loading)	3.46×10^{-6}	100 (static)	346	382
1 (dynamic loading)	3.46×10^{-6}	80 (dynamic)	276	305
2 (static loading)	2.00×10^{-5}	85 (static)	1700	1880
2 (dynamic loading)	2.00×10^{-5}	68 (dynamic)	1360	1500

Stress, S, is equal to the torque applied at any distance from the tip, $F(L-l)$, divided by the section modulus:

$$S = \frac{F(L-l)}{\Omega}. \quad (23)$$

Substituting for Ω from Eq. 22 yields

$$S = \frac{32FL^3}{\pi D^3 (L-l)^2} = \frac{C}{(L-l)^2}, \quad (24)$$

where C is a constant term, $32FL^3/\pi D^3$. Equation 24 shows that the stress is minimized at the base and increases toward the tip. Dividing the constant term, which has units of force, by the square of the distance from the base, $(L-l)^2$, provides stress (force per unit area).

The spike will fail mechanically (break) at the place where the stress equals or exceeds a critical value, $S_{critical}$ (see Fig. 17.9). This will occur at a corresponding location designated as l_{break} (Fig. 17.9 points A and B):

$$S_{critical} = \frac{32FL^3}{\pi D^3 (L-l_{break})^2}. \quad (25)$$

Solving this equation for force yields

$$F = \frac{\pi D^3 (L-l_{break})^2 S_{critical}}{32L^3} = \kappa S_{critical}, \quad (26)$$

where $\kappa = \pi D^3 (L-l_{break})^2/(32L^3)$ and has units of area. Measurements of unbroken fossilized spikes provide nominal values for D and L of 0.066 m and 0.53 m, respectively. For the two broken spikes, designated as specimens 1 and 2 with corresponding subscripts, the values of l_{break} are 0.395 m and 0.205 m, respectively. The constant κ thus has a unique value for each of these specimens:

$$\kappa_1 = 1.896 \cdot 10^{-4} \cdot (0.53-0.395)^2 = 3.46 \cdot 10^{-6} m^2 \quad (27a)$$
$$\kappa_2 = 1.896 \cdot 10^{-4} \cdot (0.53-0.205)^2 = 2.00 \cdot 10^{-5} m^2. \quad (27b)$$

Finally, the value of $S_{critical}$ must be estimated for each of the two broken specimens. The porosity of specimen 1 at its break point is 11 percent, and that of specimen 2 is 16 percent (porosity is estimated from

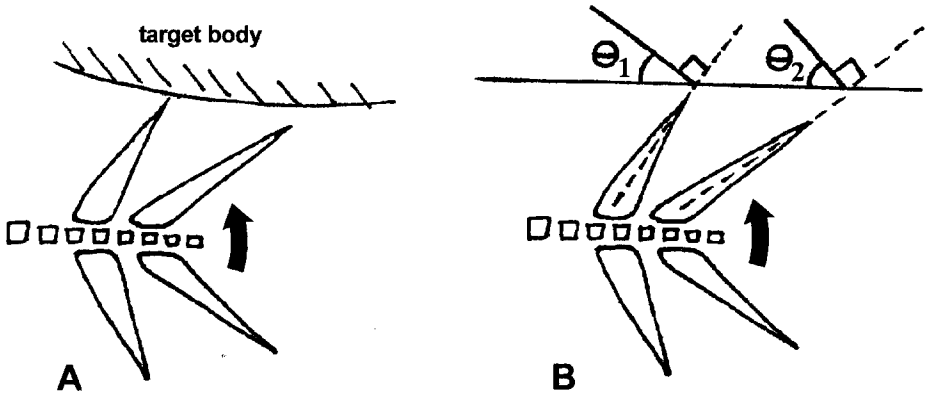

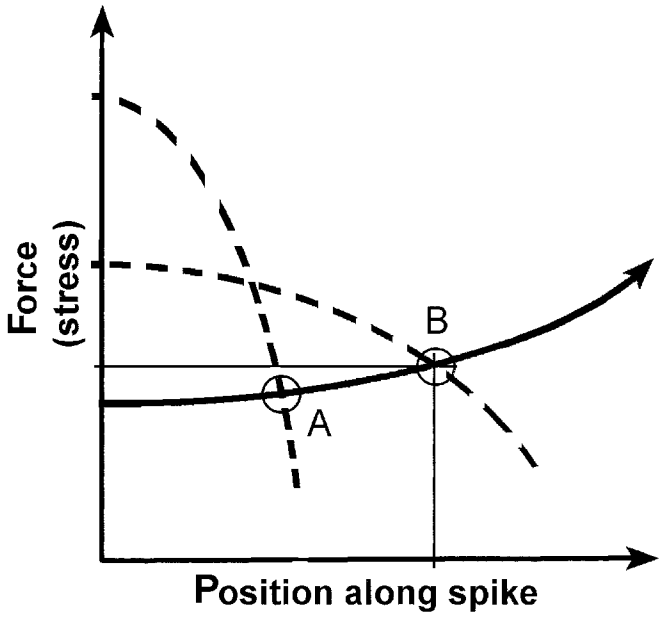

Figure 17.8. (above) The spike impact geometry is idealized from an actual impact. (A) A case in which a predator's body is parallel to the Stegosaurus. *The* Stegosaurus *tail strikes the target body with maximum possible force, just as it crosses the animal's medial axis. (B) The geometry is simplified. The angle θ between the total impact force and the component that may break the spike (see Fig. 17.9) varies depending upon whether a spike is anterior or posterior and upon the exact orientations of the animals' bodies; the angle is on the order of 25°.*

the normal spike, DMNH 1483). Based upon the characteristics of modern bone, the static failure stress values for these porosities are as shown in Table 17.8. Failure under dynamic loading (which is more realistic for a *Stegosaurus* spike impact) is expected to occur at about 80 percent of these values, as noted in Table 17.8. In Table 17.8, the necessary applied force to cause mechanical spike failure at the observed lengths is computed from Eqs. 26 and 27.

The total dynamically applied force required to break the first specimen (Figs. 17.3B, 15.7A) at the observed length of 39.5 cm from the base (with the observed 11 percent porosity value at that point) is 305 N. This is well within the minimum available impact force of 360 N computed above. Even the statically applied force that would be required is close to that limit.

Figure 17.9. Bending stresses exerted on spike of length L *at the moment of impact as a function of position along the length of the bone. Minimum stress value* C *(described in text) occurs at the base and increases as the square of the distance from the base. The bone will break at position A or B, which corresponds to* l_{break} *for the specimens; this is where the stress level equals* $S_{critical}$. *The curve showing stress required to break the spike is schematic only.*

For the second specimen, with the observed value of 16 percent porosity at its break point of only 20.5 cm from the base (Figs. 17.3A, 17.7A), the dynamically applied force at the tip would have to be about 1500 N. This is three times the 510-N maximum impact force limit computed above, implying that the mechanism of direct impact could not have caused this spike to break at the observed location.

The break observed on specimen 1 could have been caused by a slashing impact on a predator's body (fig. 17.8). The required force value of 305 N for dynamic force required to generate the break compares favorably with the minimum computed impact force of 360 N. Therefore, the damage observed in specimen 1 was probably caused by an impact at slightly less than the minimum theoretical force, in a geometry where the impact force was nearly at right angles to the spike's longitudinal axis (fig. 17.9). This further implies that the *Stegosaurus* and its predator were roughly parallel to each other when the impact occurred, and that the *Stegosaurus* tail struck when it was approximately aligned on the medial line of the animal's body.

The break observed on specimen 2, which at 1500 N of dynamic loading required three times the maximum possible computed force of 510 N, could not have been generated by spike impact. The only remaining likely possibility is that this spike struck not with the slashing action of specimen 1 but rather with a stabbing action in which the main force of impact was directed along the spike's longitudinal axis and in which the spike ultimately lodged somewhere in the predator's skeleton. When the two animals twisted apart, the spike would likely have been broken at the high force level we have computed. Evidence that such events did occur is seen by the pierced *Allosaurus* vertebra (Fig. 17.1) and a possible puncture in an *Allosaurus* pubis (Bruce Rothschild, pers. comm.).

Conclusions

Antagonistic interaction between *Allosaurus,* a predator, and *Stegosaurus,* a potential prey animal, has long been hypothesized, but only recently has evidence for this interaction been found. A bitten cervical plate of *Stegosaurus* shows that *Allosaurus* did attack *Stegosaurus* and, in at least one instance, did target the neck. Furthermore, a punctured caudal vertebra of *Allosaurus* and broken tail spikes show that *Stegosaurus* did use its spikes as weapons against *Allosaurus.* These occurrences demonstrate that there were frequent interactions between these two antagonists, probably as predator and prey.

The two broken spikes, specimens 1 and 2, apparently represent two ways in which *Stegosaurus* spikes were used as weapons. The first injury, caused by the slashing-action impact when the predator attempted to attack with its body parallel to the *Stegosaurus,* might be expected to have occurred more commonly. The second type of injury, caused when the spike piercing the tissue of the attacker, would be less likely, owing to the more difficult geometry of impact. But it would potentially cause the most serious injuries for both predator and prey because the spearing action could deeply embed the spike somewhere in

the predator's skeleton. The resulting break when the two animals disengaged would have left the predator with a large piece of spike stuck in its body and the *Stegosaurus* with a gaping wound on its tail, because the spike would have broken close to the base. Secondary infections in both animals would likely have ultimately killed both of them, if they survived their immediate encounter.

Both of the force values estimated for breaking the spikes are well within the range of computed values that could be exerted during the impact of a *Stegosaurus* spike into a target. This analysis and the observed breakage *Stegosaurus* spikes indicate that the problem with the use of these defensive weapons was not in generating enough force to penetrate the tissues of a predator but rather in restricting the off-axis impact forces to values small enough to prevent spike breakage, either on impact or subsequent to impact as the spikes were wrenched out of predators' soft tissues or bony parts.

Acknowledgments. We thank Kenneth Stadman, Earth Science Museum, Brigham Young University, Provo, Utah, and Mike Getty and Scott Sampson, Utah Museum of Natural History, Salt Lake City, Utah, for access to the *Allosaurus* specimen. We also thank Thomas Barsch, M.D., Radiology Department, Kaiser Permanente, Denver, Colorado, for discussions on the reactive bone pathology and Bruce Rothschild for discussions about the *Allosaurus* pathology. Finally, special thanks to David Fyhrie, Galateia Kazakia, John Cotton, James Funk, and John Currey for discussions about how to solve the problem of *Stegosaurus* tail spike breakage at different points.

References Cited

Boucot, A. J. 1990. *Evolutionary Paleobiology of Behavior and Coevolution.* Amsterdam: Elsevier Publishers.

Buffetaut, E. 1983. Wounds on the jaw of an Eocene mesosuchian crocodilian as possible evidence for the antiquity of crocodilian intraspecific fighting behaviour. *Paläontologische Zeitschrift* 57: 143–145.

Carpenter, K. 1997. Agonistic behavior in pachycephalosaurs (Ornithischia: Dinosauria): A new look at head-butting behavior. *Contributions to Geology, University of Wyoming* 32: 19–25.

Carpenter, K. 1998a. Armor of *Stegosaurus stenops,* and the taphonomic history of a new specimen from Garden Park, Colorado. In K. Carpenter, D. Chure, and J. I. Kirkland (eds.), *The Morrison Formation: An Interdisciplinary Study. Modern Geology* 23: 127–144.

Carpenter, K. 1998b. Evidence of predatory behavior by carnivorous dinosaurs. In B. P. Pérez-Moreno, T. Holtz Jr., J. L. Sanz, and J. Moratalla (eds.), *Gaia: Aspects of Theropod Paleobiology,* vol. 15: 135–144. Lisbon: Museu Nacional de História Natural.

Chiappe, L. M., L. Salgado, and R. A. Coria. 2001. Embryonic skulls of titanosaur sauropod dinosaurs. *Science* 293: 2444–2446.

Clarke, J. M., M. A. Norell, and L. M. Chiappe. 1999. An oviraptorid skeleton from the late Cretaceous of Ukhaa Tolgod, Mongolia, preserved in an avian-like brooding position over an oviraptorid nest. *American Museum Novitates,* no. 3265: 1–36.

Cott, H. B. 1961. Scientific results of an inquiry into the ecology and economic status of the Nile Crocodile (*Crocodilus niloticus*) in Uganda

and Northern Rhodesia. *Transactions of the Zoological Society of London* 29: 211–357.

Currey, J. D. 2002. *Bones: Structure and Mechanics.* Princeton, N.J.: University of Princeton Press.

Currie, P. J., and P. Dodson. 1984. Mass death of a herd of ceratopsian dinosaurs. In W.-E. Reif and F. Westphal (eds.), *Third Symposium on Mesozoic Terrestrial Ecosystems: Short Papers,* pp. 61–66. Tübingen: Attempto Verlag.

Erickson, G. M., and K. H. Olson. 1996. Bite marks attributable to *Tyrannosaurus rex:* Preliminary description and implications. *Journal of Vertebrate Paleontology* 16: 175–178.

Erickson, G. M., S. D. Van Kirk, J. Su, M. E. Levenston, W. E. Caler, and D. R. Carter. 1996. Bite-force estimation for *Tyrannosaurus rex* from tooth-marked bones. *Nature* 382: 706–708.

Farlow, J., C. Thompson, and D. Rosner. 1976. Plates of the dinosaur *Stegosaurus:* Forced convection heat loss fins? *Science* 192: 1123–1125.

Fick, R. 1910. *Handbuch der Anatomie und Meckanik der Gelenke Unter Berücksichtigung der bewegenden Muskeln.* Jena: Fischer.

Galton, P. M. 1973. The cheeks of ornithischian dinosaurs. *Lethaia* 6: 67–89.

Gatsey, S. M. 1990. Caudofemoral musculature and the evolution of theropod locomotion. *Paleobiology* 16: 170–186.

Glasstone, S., and P. J. Dolan. 1977. *The Effects of Nuclear Weapons.* Washington, D.C.: U.S. Department of Defense and U.S. Department of Energy.

Horner, J. R. 1997. Behavior. In P. J. Currie and K. Padian (eds.), *Encyclopedia of Dinosaurs,* pp. 45–50. San Diego: Academic Press.

Ikai, M., and T. Fukunaga. 1968. Calculation of muscle strength per unit cross-sectional area of human muscle by means of ultrasonic measurement. *Internationale Zeitschrift für Angewandte Physiologie Einschlägig Arbeitsphysiologie* 26: 26–32.

Kreighbaum, E., and K. Barthels. 1985. *Biomechanics: A Qualitative Approach for Studying Human Movement.* Minneapolis: Burgess Publishing Co.

McWhinney, L., B. Rothschild, and K. Carpenter. 2001. Posttraumatic chronic osteomyelitis in *Stegosaurus* dermal spikes. In K. Carpenter (ed.), *The Armored Dinosaurs,* pp. 141–156. Bloomington: Indiana University Press.

Myhrvold, N., and P. J. Currie. 1997. Supersonic sauropods? Tail dynamics in the diplodocids. *Paleobiology* 23: 393–409.

Thulborn, T. 1993. Mimicry in ankylosaurid dinosaurs. *Records of the South Australian Museum* 27: 151–158.

Witmer, L. M. 1995. The extant phylogenetic bracket and the importance of reconstructing soft tissues in fossils. In J. J. Thomason (ed.), *Functional Morphology in Vertebrate Paleontology.* Cambridge: Cambridge University Press.